Journal of Nonlinear Optical Physics & Materials
Vol. 26, No. 1 (2017) 1750014 (10 pages)

DOI: 10.1142/S021886351750014X

World Scientific
www.worldscientific.com

Bandwidth analysis of non-collinear fourth and fifth harmonic generation in nonlinear uniaxial crystals

Dongsheng Song, Yuanlin Zheng, Xiaohui Zhao,
Zengyan Cai and Xianfeng Chen*

State Key Laboratory of Advanced Optical Communication Systems and Networks,
School of Physics and Astronomy, Shanghai Jiao Tong University,
800 Dongchuan Road, Shanghai 200240, P. R. China

Key Laboratory for Laser Plasma (Ministry of Education),
Collaborative Innovation Center of IFSA (CICIFSA),
Shanghai Jiao Tong University,
800 Dongchuan Road, Shanghai 200240, P. R. China
**xfchen@sjtu.edu.cn*

Received 23 February 2014

The optimal angle bandwidth and wavelength bandwidth of fourth-harmonic generation (FHG) and fifth-harmonic generation (FIFHG) of the 1064 nm laser are analyzed based on the numerical calculation results of non-collinear type-I and type-II phase matching processes for general nonlinear uniaxial crystals with 1 cm length. The non-collinear phase matching angles and effective nonlinear coefficients of FHG and FIFHG are calculated. The optimal angle bandwidth and wavelength bandwidth are obtained. The results are beneficial to broadband and efficient non-collinear phase matching FHG and FIFHG experiments and studies.

Keywords: FHG; FIFHG; non-collinear phase matching; angle bandwidth; wavelength bandwidth.

1. Introduction

The broadband high efficiency fourth harmonic generation (FHG) of lasers cannot only be used as the optical probe of physical diagnostics,[1] but also has the probability of directly interacting with the nuclear target in ICF instead of third harmonic generation (THG) lasers widely used at present.[2] Shorter wavelength lasers increase the energy absorption efficiency, reduce the instability of lasers and plasmas, and suppress stimulated Brillouin scattering (SBS) and stimulated Raman scattering (SRS).[3] However, FHG can only support narrow bandwidth lasers limited by the strong dispersion properties of materials in the UV region, which makes it difficult to combine it with the present beam smoothing methods such as smoothing by

*Corresponding author.

spectral dispersion (SSD),[4] so it is necessary to study the basic theory and develop key technologies of producing efficient FHG for physical applications.

Second harmonic generation (SHG) and THG have been widely studied to get ultrashort and ultra-intense lasers, and many effective technology methods have been used for the phase matching of broadband pulses, such as achromatic phase matching,[5] chirp matched harmonic generation,[6] multi-crystals design,[7] quasi phase matching,[8] retracing point phase matching,[9] etc. However, the non-collinear phase matching technology is relatively a new study direction for its free geometry configuration,[10] and it can be used in the prefocusing scheme to get higher damage threshold to avoid high-power laser damage.[11] It is the primary purpose of this paper to get optimal bandwidths for a cone or parallel laser beam in the prefocusing scheme with a narrowband frequency propagating in a thin nonlinear crystal (1 cm), to find a proper material for the broadband experiment and study.

In this paper, non-collinear phase matching theory is analyzed firstly, which provides the numerical calculation foundation for non-collinear FHG and FIFHG phase matching angle (NCPMA), effective nonlinear coefficients (ENC), two kinds of angle bandwidths (AB) and wavelength bandwidth (WB) of a 1064 nm fundamental laser, using KDP as an example in Sec. 2. In Sec. 3, the optimal angle bandwidth and wavelength bandwidth and the corresponding phase matching angle and effective nonlinear coefficients are numerically calculated in the same procession as FHG of KDP for general nonlinear crystals such as DKDP, ADP, BBO, CLBO, and KBBF.

2. Non-Collinear Phase Matching Theory and Calculation in KDP Crystal

FHG and FIFHG non-collinear phase matching theory is similar to SHG or THG, which can all be described by the three-wave coupled equation.[12] There are two methods to get FHG 226 nm (4ω) laser, one is sum-frequency generation (SFG) of a fundamental wave of 1064 nm (ω) and its third harmonic wave 355 nm (3ω) ($\omega + 3\omega \rightarrow 4\omega$), the other is SHG of a 532 nm (2ω) laser ($2\omega + 2\omega \rightarrow 4\omega$). Both methods are calculated in type-I ($o + o \rightarrow e$) and type-II ($e + o \rightarrow e$) in this paper. Meanwhile, the two methods for the FIFTH 213 nm (5ω) laser are SFG of a 1064 nm (ω) laser and a 226 nm laser ($\omega + 4\omega \rightarrow 5\omega$), or SFG of a 532 nm laser and a 355 nm laser ($2\omega + 3\omega \rightarrow 5\omega$) with two types same as the FHG. The NCPMA, ENC, AB and WB are calculated for the KDP crystal with 1 cm.

The calculation of angle bandwidth is based on two schemes. In scheme one, the two inject waves are both cone beams, and in scheme two the first beam is parallel, and the second beam is cone. These two schemes are both useful for the prefocusing scheme used to avoid high power laser focusing damage.[11]

2.1. *Non-collinear phase matching angle*

The geometry configuration of non-collinear phase matching has been analyzed in Ref. 13. The following equations are used to calculate the type-I phase matching angles for a given exit angle θ_3,

$$\left(\frac{n_1\omega_1}{c}\right)^2 + \left(\frac{n_3(\theta_3)\omega_3}{c}\right)^2 - \left(\frac{n_2\omega_2}{c}\right)^2 = 2\frac{n_1\omega_1}{c}\frac{n_3(\theta_3)\omega_3}{c}\cos(\theta_3-\theta_1), \tag{2.1}$$

$$\left(\frac{n_2\omega_2}{c}\right)^2 + \left(\frac{n_3(\theta_3)\omega_3}{c}\right)^2 - \left(\frac{n_1\omega_1}{c}\right)^2 = 2\frac{n_2\omega_2}{c}\frac{n_3(\theta_3)\omega_3}{c}\cos(\theta_2-\theta_3), \tag{2.2}$$

where θ_1, θ_2 and θ_3 are, respectively, the angle between z axis and three waves. For type-II, the equations are almost the same, except that n_1 is an extraordinary light and should be replaced by $n_1(\theta_1)$. For KDP crystal, the phase matching angles for FHG by non-collinear mixing the fundamental wave at 1064 nm and the third harmonic wave at 355 nm are numerically calculated by the above equations. Two types of phase matching angle relationship curves are shown in Fig. 1.

In Fig. 1(a) for type-I, the region of θ_3 satisfying the non-collinear phase matching condition is from 59.95° to 120.05°, and there are two pairs of θ_1 and θ_2 for each given θ_3. The blue pair of curves is for $\theta_1 < \theta_3 < \theta_2$ and the red pair is for $\theta_1 > \theta_3 > \theta_2$. Points A and B, $\theta_1 = \theta_3 = \theta_2$, represent the collinear phase matching angles for type-I. Similarly, the region of θ_3 is from 72.03° to 107.97° for type-II in Fig. 1(b). The collinear phase matching angle is marked as point E, but meanwhile, for this θ_3 at point E, there is another θ_1 and θ_2 fitting the non-collinear triangle. However, at points C and D, there is only one non-collinear phase matching situation, while point C is for θ_2 and point D is for θ_1. Similar to type-I, the blue pair is for $\theta_1 < \theta_3 < \theta_2$ and the red pair is for $\theta_1 > \theta_3 > \theta_2$. The two pairs are center symmetry with each other about the point of (90°, 90°) in both figures, because of the axis symmetry of the uniaxial crystal. The phase matching angle region of type-I is bigger than type-II, the same situation also happens in other crystals calculated in Sec. 3. This provides a convenient condition for the experiment.

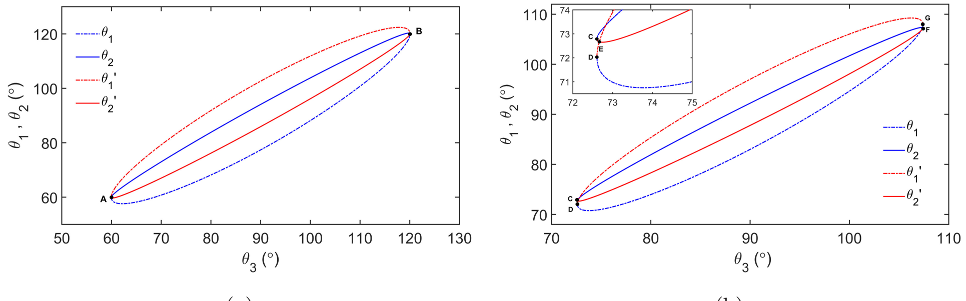

(a) (b)

Fig. 1. FHG NCPMA. The blue curve is for $\theta_1 < \theta_3 < \theta_2$, the red curve is for $\theta_1 > \theta_3 > \theta_2$. (a) Type-I. Point A and B represent the collinear point. (b) Type-II. Point E represents the collinear point, Point C and D represent the smallest value of θ_2 and θ_1 fitting non-collinear condition.

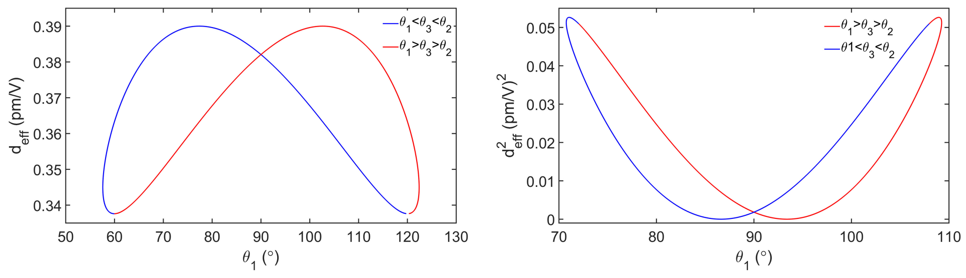

(a) (b)

Fig. 2. (a) Type-I FHG ENC of KDP. (b) Type-II FHG ENC of KDP.

2.2. *Effective nonlinear coefficients*

The ENC for the nonlinear crystals is distinguished by the point group they belong to. The expression for different point group may be different.[14] The non-collinear ENC is more complex than the collinear situation. For KDP belonging to $\bar{4}2m$ point group, the expression is $d_{\mathrm{eff}} = -d_{36} \sin\theta_3 \sin 2\varphi$ for type-I and $d_{\mathrm{eff}} = d_{14} \sin\theta_1 \cos\theta_3 \cos 2\varphi + d_{36} \cos\theta_1 \sin\theta_3 \cos 2\varphi$ for type-II. ENC for FHG type-I d_{eff} and FHG type-II d_{eff}^2 — the square index is eliminating the negative value appearing in type-II — is calculated and shown in Figs. 2(a) and 2(b) respectively based on the numerical calculation results of the FHG phase matching angles for KDP crystal. The blue curve represents $\theta_1 < \theta_3 < \theta_2$ and the red curve represents $\theta_1 > \theta_3 > \theta_2$. For type-I, the ENC of $\theta_1 < \theta_3 < \theta_2$ matching type is bigger when $\theta_1 < 90°$, so it should be chosen to get higher conversion efficiency. It should choose the $\theta_1 > \theta_3 > \theta_2$ matching type for type-II for the same reason. Overall, the ENC of type-I is much larger than that of type-II.

2.3. *Angle bandwidth*

According to the relationship of the conversion efficiency and phase mismatching factor on the conditions of slowly varying amplitude approximation and small signal approximation, one can easily define the bandwidth of angle or wavelength. Meanwhile, the phase matching factor can be expressed as

$$\Delta k = \Delta k_0 + \left.\frac{\partial(\Delta k)}{\partial\theta}\right|_{\theta=\theta_m} \Delta\theta + \left.\frac{\partial(\Delta k)}{\partial\lambda}\right|_{\lambda=\lambda_0} \Delta\lambda + \cdots, \tag{2.3}$$

where θ_m is the phase matching angle, and λ_0 is the center wavelength of the beam.

Two kinds of schemes mentioned in Sec. 2.1 are calculated for each set of θ_1, θ_2, θ_3. In scheme one the two inject beams are cone beams, where the edge-ray can be considered as the center beam rotates by a small angle. Because every ray of $\vec{k}_1$ with a small departure angle from the center ray must has a corresponding ray of $\vec{k}_2$ with the same departure angle, the geometry relationship between the two departure rays is the same as the center rays (Fig. 3(a)). While in scheme two the first fundamental beam is a parallel light, and the second fundamental beam is a

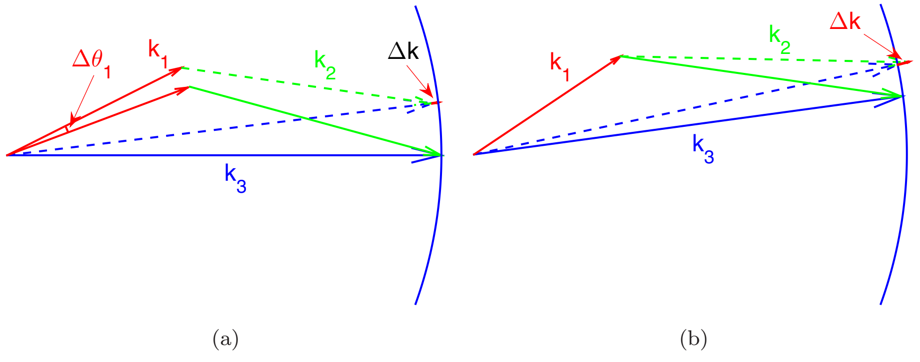

Fig. 3. Two kinds of angle bandwidth scheme. (a) $\vec{k}_1$ and $\vec{k}_2$ are both cone beams and (b) $\vec{k}_1$ is cone and $\vec{k}_2$ is parallel.

cone beam, in this situation, the changing of θ_2 causes the phase mismatching. The schematic diagrams for the angle bandwidth of the two institutions are shown in Fig. 3, separately.

Figure 4 shows the numerical calculation results of the angle bandwidth versus θ_3 for KDP crystal. For type-I (the dash-dotted curves), the blue curve shows that the angle bandwidth has the maximum value of $\Delta\theta_1 = 1.813°$ at the non-critical angle of $\theta_3 = 90°$ for the cone inject beams. The red one shows that the first fundamental beam is parallel and the second fundamental beam is cone. It shows that the maximum value is $\Delta\theta_2 = 0.9935°$ at the minimal value of θ_1 when $\theta_3 = 62.2°$. Meanwhile, for type-II (the solid curves), the angle of the maximum value is a little larger than that from type-I for cone beams, and the maximum angle bandwidth is 1.9897° when $\theta_3 = 91.02°$, which is 0.9776° for the other matching situation when $\theta_3 = 73.77°$. The situation is almost the same for other crystals mentioned below.

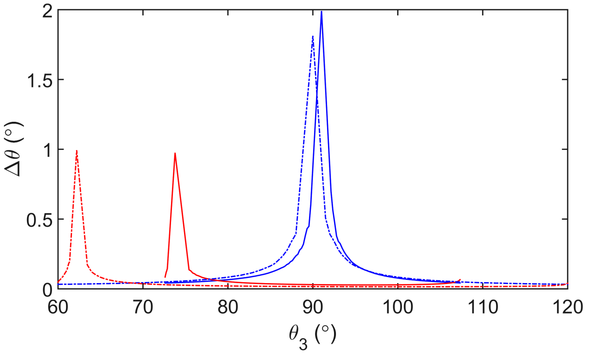

Fig. 4. Non-collinear FHG angle bandwidth of scheme one (blue curves) and scheme two (red curves) with type-I (dash-dotted curves) and type-II (solid curves) for KDP.

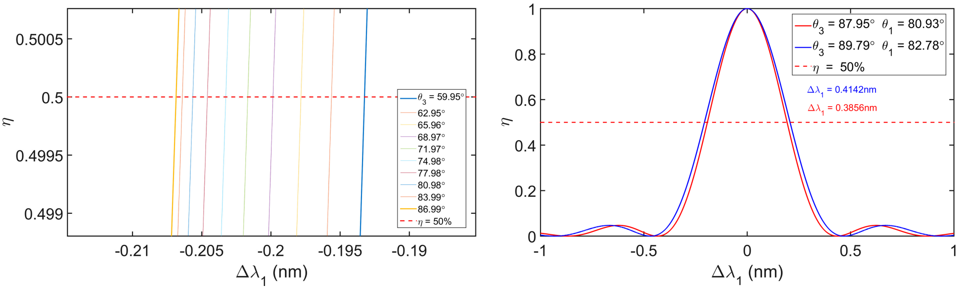

(a) (b)

Fig. 5. FHG Wavelength bandwidth for KDP. (a) Wavelength bandwidth region. (b) The maximum wavelength bandwidths for type-I (blue curve) and type-II (red curve).

2.4. *Wavelength bandwidth*

With the frequency relationship between the three beams, $\Delta\omega_2 = 2\Delta\omega_1$, $\Delta\omega_3 = 3\Delta\omega_1$, we have $\Delta\lambda_2 = -\frac{\lambda_2^2}{2\pi c}\Delta\omega_2 = -\frac{\lambda_1^2}{8\pi c}2\Delta\omega_1 = -\frac{1}{2}\frac{\lambda_1^2}{2\pi c}\Delta\omega_1 = \Delta\lambda_1/2$ and $\Delta\lambda_3 = \Delta\lambda_1/3$. Figure 5 shows the numerical calculation results based on the definition of wavelength bandwidth in Eq. (2.3). Figure 5(a) evidences that the wavelength bandwidth for type-I has the maximum value around the uncritical angle, shown as the yellow line, and the range of half wavelength bandwidth for all the possible phase matching situation is within about 0.012 nm for the KDP crystal, shown as the lines in the region between the yellow line and blue line. Figure 5(b) shows the maximum wavelength bandwidths for type-I (the blue curve) and type-II (the red curve), they are more or less equal to each other, which evidences that the phase matching situation has almost no influence on the WB. The situation is almost the same for other crystals mentioned in Sec. 3.

3. Calculation in Other Crystals and Discussion

We calculate the NCPMA, ENC, optimal AB and WB for FHG and FIFHG of other usual uniaxial crystals in the same method as for the KDP crystal in Sec. 2. These crystals are DKDP, ADP, BBO, $BeSO_4{\cdot}4H_2O$, DADP, ADA, DADA, CLBO, KABO, BABF, KBBF, LB4. They are selected for two reasons, one is that their transparencies include the FHG and FIFHG of a 1064 nm laser,[15,16] the other is that the non-collinear phase matching condition can be satisfied. The results are shown in Tables 1 and 2. Not all crystals calculated are mentioned in the table but the ones with the best performance in one or two items are mentioned. Table 1 shows type-I non-collinear phase matching results, and Table 2 shows type-II non-collinear phase matching results. Each table contains the angle bandwidth for the cone beams (ABCC), the angle bandwidth for the first beam is parallel and the second beam is cone (ABPC), wavelength bandwidth (WB), the corresponding non-collinear phase matching angle (NCPMA) and effective nonlinear coefficient (ENC).

Table 1. Calculation results for type-I.

Crystal	Scheme	ABCC (°)	NCPMA (°/°)[a]	ENC (pm/V)	ABPC (°)	NCPMA (°/°)	ENC (pm/V)	WB (nm)	NCPMA (°/°)	ENC (pm/V)
KDP	4(1+3)[b]	1.8128	90/77.37	0.39	0.9935	62.21/57.59	0.3450	0.4142	89.79/77.16	0.3900
	4(2+2)	1.8122	90/86.69	0.39	0.8801	77.03/76.25	0.3800	0.148	90/86.69	0.3900
DADP	4(1+3)	1.7876	90/77.29	0.43	0.9883	62.35/47.68	0.3809	0.4006	89.79/77.08	0.4300
	4(2+2)[c]	1.7888	90/87.27	0.43	0.8761	79.45/78.79	0.4227	0.13938	90/87.27	0.4300
	5(1+4)[d]	1.4685	90/86.13	0.43	0.8851	83.89/82.03	0.4275	0.2011	90.05/86.19	0.4300
BBO	4(1+3)	1.0978	90/58.33	0.16	0.9585	47.87/32.64	1.661	0.2759	89.15/57.49	0.1941
	4(2+2)	1.0978	90/74.41	0.16	0.8400	50.01/45.21	1.601	0.09055	90/74.41	0.1600
	5(1+4)	0.8996	90/57.34	0.16	0.9025	60.50/40.71	1.272	0.1091	90.81/58.17	0.1275
	5(2+3)	0.8994	90/79.37	0.16	0.7028	71.86/67.03	0.8681	0.06383	90.17/79.54	0.1532
$BeSO_4 \cdot 4H_2O$	4(1+3)	1.9172	90/78.88	0.23	1.0061	64.45/60.49	0.2075	0.3856	89.81/78.69	0.2300
	4(2+2)	1.9172	90/87.98	0.23	0.8915	81.76/81.31	0.2276	0.1396	90/87.98	0.2300
CLBO	4(1+3)	1.642	90/72.08	0.74	1.1124	53.78/47.12	0.7422	0.3716	89.84/71.92	0.7400
	4(2+2)	1.6421	90/82.36	0.74	0.888	62.34/60.50	0.6554	0.13349	90/82.36	0.7400
	5(1+4)	1.386	90/76.98	0.74	0.8992	70.59/64.20	0.6979	0.156	90.31/77.28	0.7400
KBBF	4(1+3)	1.4472	90/61.81	0	1.111	36.05/26.83	0.3962	0.6866	88.74/60.56	0.0108
	4(2+2)	1.4473	90/75.00	0	0.9239	37.91/34.85	0.3866	0.2399	90/75.00	0
	5(1+4)	1.2691	90/59.08	0	1.0281	43.91/30.65	0.3530	0.3702	91.34/60.43	0.0115
	5(2+3)[e]	1.2695	90/74.25	0	0.8186	49.57/44.84	0.0778	0.2275	90.48/74.74	0.0010

Note:
[a] (θ_3/θ_1).
[b] 4(1+3): $\omega + 3\omega \rightarrow 4\omega$.
[c] 4(2+2): $2\omega + 2\omega \rightarrow 4\omega$.
[d] 5(1+4): $\omega + 4\omega \rightarrow 5\omega$.
[e] 5(2+3): $2\omega + 3\omega \rightarrow 5\omega$.

Table 2. Calculation results for type-II.

Crystal	Scheme	ABCC (°)	NCPMA (°/°)[a]	ENC (pm/V)	ABPC (°)	NCPMA (°/°)	ENC (pm/V)	WB (nm)	NCPMA (°/°)	ENC (pm/V)
KDP	4(1+3)[b]	1.9898	91.09/84.06	0.0330	0.9776	73.77/70.75	0.2264	0.3857	87.96/80.93	0.0751
DADP	4(1+3)	2.004	90.85/85.91	0.0243	0.9687	78.22/75.92	0.1875	0.395	89.89/84.80	0.0398
BBO	4(1+3)	1.1957	93.88/66.83	0.06124	0.936	52.02/36.95	1.131	0.277	90.86/63.42	0.0154
	4(2+2)[c]	1.4382	90.84/87.99	0.0012	0.8113	81.16/79.67	0.0634	0.0874	89.80/86.87	0.0004384
	5(1+4)[d]	0.9271	86.79/58.28	0.0677	0.7895	64.06/44.92	0.7124	0.1074	90.77/62.48	0.01428
$BeSO_4 \cdot 4H_2O$	4(1+3)	2.149	90.19/89.09	0.0029	0.9865	87.29/86.80	0.2368	0.3698	89.68/88.57	0.0070
CLBO	4(1+3)	1.8289	92.10/79.37	0.1098	0.9921	62.39/56.58	0.6474	0.3856	89.62/76.73	0.1746
KBBF	4(1+3)	1.6267	94.31/70.59	0.01224	1.0870	40.56/30.90	0.3194	0.7532	97.50/74.25	0.01736
	4(2+2)	2.0014	92.44/84.87	0.0019	0.9001	56.76/53.86	0.1584	0.2448	90.74/83.06	0.000765
	5(1+4)	1.3327	85.29/57.86	0.0214	1.0058	47.68/34.31	0.2725	0.3876	94.77/68.03	0.01524
	5(2+3)[e]	1.5968	91.77/85.22	0.00126	0.7932	70.26/67.18	0.06419	0.2302	90.56/83.91	0.0005081

Note:
[a] (θ_3/θ_1).
[b] 4(1+3): $\omega + 3\omega \rightarrow 4\omega$.
[c] 4(2+2): $2\omega + 2\omega \rightarrow 4\omega$.
[d] 5(1+4): $\omega + 4\omega \rightarrow 5\omega$.
[e] 5(2+3): $2\omega + 3\omega \rightarrow 5\omega$.

In Table 1 for type-I, the results evidence that for ABCC, $BeSO_4 \cdot 4H_2O$ has the maximum value, but CLBO has the maximum ENC value. For ABPC, CLBO has the maximum value, while BBO has the maximum ENC value. For WB, KBBF has the maximum value, but CLBO has the maximum ENC value. Overall, for every kind of bandwidth, CLBO has bigger ENC value than most of others, KDP and DADP have the best aggregate performance.

In Table 2 for type-II, the results evidence that for ABCC, $BeSO_4 \cdot 4H_2O$ has the maximum value, but CLBO has the maximum ENC value. For ABPC, KBBF has the maximum value, while BBO has the maximum ENC value. For WB, KBBF has the maximum value, but CLBO has the maximum ENC value. Overall, for every kind of bandwidth, CLBO has bigger ENC value than most of others, KDP and DADP have the best aggregate performance.

The optimal non-collinear phase matching angle bandwidth is much bigger than that of collinear situation, while the wavelength bandwidth is more or less the same. The reason is that, for the collinear angle bandwidth, the phase matching happens at the intersection point of the $\vec{k}_1 + \vec{k}_2$ curve and $\vec{k}_3$ curve in the wave vector space, while the phase matching for the optimal bandwidth happens at the tangent point for the non-collinear situation. Therefore, the phase mismatch factor changes more slowly for the same angle changing in the latter. But for the wavelength bandwidth, there is no such tangent point as the angle wavelength. Although BBO and KBBF have bigger angle bandwidths or wavelength bandwidths, they are difficult to grow to a proper size for most applications.[17,18] CLBO has easy deliquescence in atmospheric environment.[19] Overall, KDP crystal has the best aggregate performance.

4. Conclusion

We have analyzed the theory of non-collinear phase matching for FHG and FIFHG. Two kinds of angle bandwidth configurations and one kind of wavelength bandwidth model were investigated. The phase matching angles for type-I and type-II FHG and FIFHG were numerically calculated in detail, and the maximum angle bandwidth and wavelength bandwidth were obtained for all the possible uniaxial crystals satisfying the conditions as we know so far. The results are of use to help the experimentalists choose the proper crystal and suitable configuration for non-collinear FHG or FIFHG at 1064 nm.

Acknowledgments

This work was supported in part by the National Natural Science Foundation of China Under Grant Nos. 61235009 and 11604206.

References

1. D. T. Attwood, Ultraviolet probing of laser-produced plasmas with picosecond pulses, in *Proc. SPIE 0097*, *12th Intl Congress on High Speed Photography*, 413 September 14, 1977, doi:10.1117/12.955253.

2. W. Howard Lowdermilk, Status of the national ignition facility project, in *Proc. 2nd Annual Int. Conf. SPIE 3047, Solid State Lasers for Application to Inertial Confinement Fusion*, 16, December 8, 1997, doi:10.1117/12.294296.
3. Kruer, William L, *The Physics of Laser Plasma Interactions* (Westview Press, Colorodo, 1988).
4. S. Skupsky *et al.*, Improved laser-beam uniformity using the angular dispersion of frequency-modulated light, *J. Appl. Phys.* **66**(8) (1989) 3456–3462.
5. V. D. Volosov and E. V. Goryachkina, Compensation of phase-matching dispersion in generation of nonmonochromatic radiation harmonics. I. Doubling of neodymium-glass radiation frequency under free-oscillation conditions, *Sov. J. Quantum Electron.* **6**(7) (1976) 854.
6. K. Osvay and I. N. Ross, Broadband sum-frequency generation by chirp-assisted group-velocity matching, *JOSA B* **13**(7) (1996) 1431–1438.
7. D. Eimerl, Quadrature frequency conversion, *IEEE J. Quantum Electron.* **23**(8) (1987) 1361–1371.
8. A. M. Schober, M. Charbonneau-Lefort and M. M. Fejer, Broadband quasi-phase-matched second-harmonic generation of ultrashort optical pulses with spectral angular dispersion, *JOSA B* **22**(8) (2005) 1699–1713.
9. M. S. Webb, D. Eimerl and S. P. Velsko, Wavelength insensitive phase-matched second-harmonic generation in partially deuterated KDP, *JOSA B* **9**(7) (1992) 1118–1127.
10. N. Boeuf *et al.*, Calculating characteristics of non-collinear phase matching in uniaxial and biaxial crystals, *Opt. Eng.* **39**(4) (2000) 1016–1024.
11. J. Chen *et al.*, Noncollinear third-harmonic generation with large angular acceptance by noncritical phase matching in KDP crystal, *Opt. Lett.* **40**(19) (2015) 4484–4487.
12. Y.-R. Shen, *The Principles of Nonlinear Optics* (Wiley-Interscience, New York, 1984), pp. 575.
13. H. J. Liu *et al.*, Phase matching analysis of non-collinear optical parametric process in nonlinear anisotropic crystals, *Opt. Commun.* **197**(4) (2001) 507–514.
14. R. W. Boyd, *Nonlinear Optics*, *Handbook of Laser Technology and Applications* (Three-Volume Set) (Taylor & Francis, Oxfordshire, 2003), pp. 161–183.
15. D. N. Nikogosyan, *Nonlinear Optical Crystals*: *A Complete Survey* (Springer Science & Business Media, Germany, 2006).
16. V. G. Dmitriev, G. G. Gurzadyan and D. N. Nikogosyan, *Handbook of Nonlinear Optical Crystals*, Vol. 64 (Springer, Germany, 2013).
17. A. E. Kokh *et al.*, Growth and investigation of BBO crystals with improved characteristics for UV harmonic generation, in *Proc. Laser Material Crystal Growth and Nonlinear Materials and Devices*, Vol. 3610 (1999) 139–147.
18. C. T. Chen *et al.*, Deep-UV nonlinear optical crystal KBe 2 BO 3 F 2discovery, growth, optical properties and applications, *Appl. Phys. B*: *Lasers Optics* **97**(1) (2009) 9–25.
19. F. Pan *et al.*, Cracking mechanism in CLBO crystals at room temperature, *J. Crystal Growth* **241**(1) (2002) 129–134.